

Understanding the solution dynamics and binding of PVDF binder with silicon, graphite, and NMC materials and the influence on cycling performance

Mary K. Burdette-Trofimov[†], Beth L. Armstrong^{*,‡}, Rachel J. Korkosz[†], J. Landon Tyler[†], Rebecca D. McAuliffe[†], Luke Heroux[¶], Mathieu Doucet[¶], David T. Hoelzer[‡], Nihal Kanbargi[†], Amit K. Naskar[†], and Gabriel M. Veith^{*,†}

[†]Chemical Sciences Division, Oak Ridge National Laboratory

[‡] Materials Science and Technology Division, Oak Ridge National Laboratory

[¶]Neutron Scattering Division, Oak Ridge National Laboratory

E-mail: armstrongbl@ornl.gov, veithgm@ornl.gov

ORCID

Mary K. Burdette-Trofimov: 0000-0003-2395-2867

Beth L. Armstrong: 0000-0001-7149-3576

Rachel J. Korkosz:

J. Landon Tyler: 0000-0002-5133-4567

Rebecca D. McAuliffe: 0000-0002-6497-4360

Luke Heroux: 0000-0001-8993-3904

Mathieu Doucet: 0000-0002-5560-6478

David T. Hoelzer: 0000-0001-9366-9958

Nihal Kanbargi: 0000-0002-7897-6957

Amit K. Naskar: 0000-0002-1094-0325

Gabriel M. Veith: 0000-0002-5186-4461

Keywords

Silicon anode, binder, electrode processing, PVDF, battery electrode

Abstract

The impact of the binding, solution structure and solution dynamics of Poly(vinylidene fluoride) (PVDF) with silicon on its performance as compared to traditional graphite and $\text{Li}_{1.05}\text{Ni}_{0.33}\text{Mn}_{0.33}\text{Co}_{0.33}\text{O}_2$ (NMC) electrode materials was explored. Through refractive index (RI) measurements the concentration of binder adsorbed on the electrode materials surface

during electrode processing was determined to be less than half of the potential available material resulting in excessive free binder in solution. Using ultra small angle neutron scattering (USANS) and small angle neutron scattering (SANS) it was found that PVDF forms a conformal coating over the entirety of the silicon particle. This is in direct contrast with graphite-PVDF and NMC-PVDF slurries where PVDF only covers part of the graphite surface, and the PVDF chains make a network-like graphite-PVDF structure. Conversely, a thick layer of PVDF covers NMC particles, but the coating is porous, allowing for ion and electronic transport. The homogeneous coating of the silicon breaks up percolation pathways resulting in the poor cycling performance of the silicon materials widely reported. These results indicate that the Si-PVDF interactions could be modified from a binder to a dispersant.

Introduction

Poly(vinylidene fluoride) (PVDF) is the binder of choice for many graphite and $\text{Li}_{1.05}\text{Ni}_{0.33}\text{Mn}_{0.33}\text{Co}_{0.33}\text{O}_2$ (NMC) based electrodes as it is electrochemically inert and flexible to enable mechanical compression-decompression cycling during charging/decharging.¹⁻³ Interestingly, electrode architectures vary widely with PVDF agglomerates organizing between graphite or NMC particles.^{4,5} The morphology of NMC/PVDF agglomerates depend on molecular weight of the PVDF.⁴ When the molecular weight of PVDF is ultra-high (~92,840,000 g/mol), the PVDF organizes around the NMC particles in thick, porous layers as confirmed with high resolution scanning electron microscopy (SEM) equipped with an energy dispersive X-ray (EDX) detector.⁴ On the other hand, when the molecular weight of the PVDF is lower (~350,000 g/mol) the PVDF on the NMC particles is a more conformal, lower porosity, coating.⁴ The decrease in porosity of the lower molecular weight PVDF

coating results in an electrode with inferior rate capability, likely due to the inhibited Li-ion diffusion, and a 50% reduction in capacity retention.⁴

In contrast, the organization of PVDF around graphite is quite different from that of NMC. Through atomic force microscopy (AFM), lateral force microscopy (LFM), and electron probe X-ray microanalysis (EPMA), it was found that PVDF only covers about 40% of the graphite surface.⁶ Additionally, PVDF chains on graphite are relatively linear, meaning that, in the slurry, the PVDF chains reach into the solvent phase and adsorb onto other graphite particles,⁶ keeping the graphite in a well-connected, conductive matrix upon cycling. While the morphology of PVDF on graphite or NMC is different (MW often not reported), both give the electrode structural stability without inhibiting electrochemical processes such as electron and ion transport.

In contrast, PVDF is generally not considered a suitable binder for silicon anodes as they typically fail after a few lithiation/delithiation cycles.⁷⁻¹⁸ Most researchers suggest the following reasons for failure: 1) poor adhesion strength between the PVDF and the silicon,¹⁹ 2) chemical degradation of PVDF during cycling, creating HF which etches the silicon,¹⁹ and 3) weak Van der Waals interactions between silicon and PVDF.^{21, 22} The focus on mechanical properties may obscure other variables. With respect to mechanical properties PVDF-based electrodes failure is often attributed to the flexibility of the PVDF which cannot withstand compressive forces during lithiation/delithiation cycles. However, Si+PVDF has a low elastic modulus of 0.57 GPa as compared to the elastic modulus of Si+sodium carboxymethylcellulose (Si+CMC) and Si+sodium alginate electrodes at 2.93 and 3.35 GPa, respectively, indicating the ability to deform elastically which should help with repeated expansions and contractions of silicon with cycling.¹⁵ In terms of compressive strength,

Si+PVDF electrodes can support about 12 MPa before the electrode experiences severe mechanical degradation as compared to Si+CMC, which can withstand 70 MPa before failure.²³ While these factors may play a role in the failure of Si+PVDF anodes, the structure of Si-PVDF slurries has not been well explored and understanding the origin of cell failure may provide insight into new approaches to stabilizing electrodes in general.

To explore the role of the multi-scale slurry structure on the performance of Si-PVDF anodes, the dynamics of Si-PVDF, graphite-PVDF, and NMC-PVDF slurries were probed with small angle neutron scattering (SANS) and ultra-small angle neutron scattering (USANS) under flow conditions. The data shows marked differences in PVDF structure with these various electrode materials leading to different binder organization upon casting and resulting cycling performances. Further, it is proposed that if the silicon surface can be modified in a way to mimic the PVDF-graphite or PVDF-NMC interaction, perhaps, PVDF could be an effective additive for silicon-based anode or other composite materials.

Experimental Section

Materials. All reagents were used without further purification unless otherwise noted. Scrap pieces, of silicon boule left over from cutting or processing into shapes, were obtained from El-Cat (Ridgefield Park, New Jersey, USA), were prepared by washing the boules sequentially in hot acetone, methanol, a 5:1:1 (v/v) mixture of DI water, NH₄OH (Fisher – Reagent Grade), and H₂O₂ (Fisher – Reagent Grade 30%). Then the boules were dipped (< 1 minute) in a 5 wt% HF solution. *Care should be taken with this procedure due to the exothermic nature of the H₂O₂ treatment and the toxicity and danger of HF.* The purpose of the treatment was to make all the silicon surfaces the same and remove cutting residue from the Si along with bits of epoxy and oil. C-ENERGY Super C45 conductive carbon black was purchased from Timcal.

Graphite (Gr, MAGE3) was purchased from Hitachi, Ltd. (Japan), and lithium nickel manganese cobalt oxide (NMC, $\text{Li}_{1.05}\text{Ni}_{0.33}\text{Mn}_{0.33}\text{Co}_{0.33}\text{O}_2$) was provided by Steward Advanced Materials (Chattanooga, TN, USA) – SEM image of the powder is shown in **Figure S1**. Solid poly(vinylidene fluoride) (PVDF), both anode (A-PVDF) and cathode grade (C-PVDF), was purchased from Kureha Corporation (Japan). N-Methyl-2-pyrrolidone (NMP, ACS grade) was purchased from Sigma Aldrich. Deuterated dimethylformamide (DMF)-D7 (D, 99.5%) was purchased from Cambridge Isotope Laboratories, Inc. (Tewksbury, MA) for the neutron scattering experiments. Deuterated DMF is similar in polarity, structure, and functionality to NMP, and DMF-D7 is availability in quantities (and cost) required for this work.

Si fabrication was performed by attrition of silicon boules (100g, 1-3 cm in length) using a Zoz Simoloyer CM01 high energy ball mill (Wenden, Germany) equipped with 1000 g of 5 mm spherical 440C stainless steel media (Union Process). The jacket of the milling chamber was cooled with a recirculating chiller using an ethylene glycol/water mixture to 15°C. The mill was cooled for ~1 hour prior to milling. After loading the mill with silicon boule fragments, the mill was evacuated and refilled with argon (repeat 3 times). The silicon boules were milled in argon for 90 minutes at 700 rpm. The subsequent silicon powder was collected in an argon filled jar, which was housed in an argon-filled glovebox.

Cathode grade PVDF solution (10 wt%) was prepared by adding C-PVDF to DMF-D7 (~25 g). Dissolution was completed using a Thinky planetary centrifugal mixer (PCM) equipped with 5 pieces of 5 mm 8YSZ media. Each mixing cycle consisted of mixing at 2000 rpm for 2 minutes until the C-PVDF was dissolved (approximately 12 cycles). This procedure was repeated to make 10 wt% A-PVDF in DMF-D7. To prepare Si, graphite, and NMC slurries for neutron

scattering, the slurry was made with the following order of addition and mixing protocol using the PCM: 1) DMF-D7 (12.25 g) and milled silicon (9 g) were mixed for 2 min at 2000 rpm, and 2) the appropriate PVDF solution (10 wt% in DMF-D7) was added to the slurry and mixed for 2 min at 2000 rpm.

Characterization of Materials. The molecular weight of the C-PVDF and A-PVDF binder was determined using gel permeation chromatography (GPC) with an Agilent 1100 series Autosampler (1313A), quaternary pump, vacuum degasser, column oven (Waters Temperature Control Module II), and a flow-cell refractive index detector (ERC RefractoMax520). Both the columns (Jordi polystyrene mixed bed column with molecular range 500 to 2,000,000 g/mol) and the refractive index detector were heated to 35°C.

C-PVDF and A-PVDF were dissolved in HPLC grade NMP (5 g/mL, Sigma Aldrich) for a minimum of 24 hours prior to filtration and injection. The solution was filtered through a 0.2 µm PTFE syringe filter prior to injection (40 µL) where the eluent was HPLC grade NMP, and the flow rate was 0.75 mL/min. Chromatograms were evaluated with Agilent ChemStation software.

Refractive Index (RI) Measurements: Refractive index was measured on a Mettler Toledo RM40 Refractometer. Twelve solutions of C-PVDF and A-PVDF in NMP (0.25 wt% to 10 wt%) were measured using the refractometer to create a calibration curve. For binder absorption measurements a series of silicon, NMC, or graphite (2 g) slurries containing 0.25 wt% to 10 wt% (with respect to active material) of C-PVDF, for NMC, or A-PVDF, for silicon and graphite, were made. These slurries were shaken on a rocker table for 1 week in the dark to ensure complete adsorption. The slurries were subsequently centrifuged at 6000 rpm for 30 minutes, the supernatant was removed, and its refractive index was measured. As a control, a 10 wt% solution without

electrode material was centrifuged and the supernatant analyzed. The RI data showed no change indicating the PVDF was well dispersed in solution.

Brunauer–Emmet–Teller (BET) Surface Area Analysis: Nitrogen adsorption and desorption experiments were performed on a Quantachrome Autosorb iQ at 77 K. The Brunauer–Emmet–Teller (BET) model of isotherms was utilized, and the adsorption of N₂ at small relative pressures was fit to calculate surface area of each sample.²⁴ Approximately 150 mg of sample was loaded into a 9.0 mm cell. The sample was degassed at a rate of 2°C/min to 300°C for 12 hours. After degassing, the cell volume was replaced with helium and re-weighed. The sample was analyzed in the BET using a P/P₀ range of 0.0002 to 0.99.

Neutron scattering measurements were obtained at the Spallation Neutron Source (SNS) at Oak Ridge National Laboratory (ORNL). For all scattering measurements, the neutron scattering intensity is measured as a function of Q, the neutron wave vector transfer as shown by Equation 1, where θ is the scattering angle, and λ represents the neutron wavelength.²⁵ Raw data were reduced using the Mantid framework to calculate I(Q).²⁶ A background measurement was performed with the empty concentric cylinder geometry using identical sampling conditions. The background measurement was subtracted from the sample measurement. Neutron data were modeled using the SasView small-angle scattering software package.²⁷

$$Q = \frac{4\pi}{\lambda} \sin\left(\frac{\theta}{2}\right) \quad \text{Eqn (1)}$$

The USANS instrument at SNS is a time-of-flight triple-bounce Bonse-Hart small-angle scattering instrument where measurements are obtained from Q= 0.0001 to 10⁻⁵ Å⁻¹.^{28, 29} All neutron scattering measurements were collected using the 3.6 Å reflection of the silicon analyzer crystals. USANS data were not normalized by intensity at Q=0 because the shape of the curve was being

fitted rather than the absolute intensity. The rheometer on the neutron scattering beamlines is an Anton Paar (Ashland, Virginia) Physica MCR501 with a quartz concentric cylinder geometry (49 mm bob and 50 mm cup). A solvent trap was used to mitigate solvent evaporation. Each rheo-USANS and rheo-EQSANS measurement was performed at a constant shear rate of 0, 30, 200, or 500 Hz. The 200 and 500 Hz shear rates represent typical shear rates used for slot die-like coaters. Hand-cast electrodes tend to be cast in the 61 to 1200 Hz range with a gap between 25-500 μm . The 30 Hz and 0 Hz shear rates correlate to the slurry being fed from the hopper to the slot die and at rest, respectively.

SANS measurements were performed using the EQSANS (Extended Q-range small angle neutron scattering) instrument at SNS.³⁰ This time-of-flight SANS instrument was used in a single configuration that allowed a wavevector transfer range between $Q=0.0055 \text{ \AA}^{-1}$ and $Q=0.11 \text{ \AA}^{-1}$, which is complementary to the USANS measurements.

Electrochemistry Measurements. Electrodes were formulated with 5 mg (0.9 mg for silicon) active material per cm^2 with a weight ratio of 10% C45 carbon black, 10% binder, and the balance electrode material. Cast electrodes were dried at 120°C for at least 12 hours and loaded into an argon filled glove box while hot. Cells were cycled in a coin cell configuration using Celgard 2325 as a separator, 1.0M LiPF_6 in 3:7 wt% ethylene carbonate:ethyl methyl carbonate (Ube) with a lithium metal counter electrode (Alfa Aesar, 0.75 mm thick ribbon). Cells were cycled at a rate of C/5 using either Biologic VMP or Maccor potentiostats at 24°C. Anodes were cycled between 0.05 and 1 V; the cathode was cycled from 3 to 4.5 V.

Results and Discussion

This work explored the role of polymer morphology on the resulting electrode performance for cells built using PVDF binder. **Figure 1** shows representative half-cell data collected over the first 10 cycles for the electrodes built from materials used in this study. The data shows the expected cycling performance, voltage plateaus, and capacities (310 mAh/g reversible for graphite and 150 mAh/g NMC). The silicon cell had a large lithiation capacity (1900 mAh/g) on the first cycle followed by a rapid loss in capacity demonstrating the negative effect of PVDF on silicon anodes. In contrast the graphite and NMC cells showed reversible cycling in the half cell configuration. **Figure 2** shows representative SEM images of the various electrodes after processing. **Figures S2, S3, and S4** show EDX data for the dried electrodes. From this data the electrodes all appear to have a homogeneous morphology and evidence for void space within/on the surface of the electrode to enable electrolyte penetration. The EDX data shows clear evidence for PVDF uniformly coating (from the homogeneous signal from the fluorine in PVDF) on the surface of the materials. To explain these differences in behavior, polymer dynamics in solution were explored.

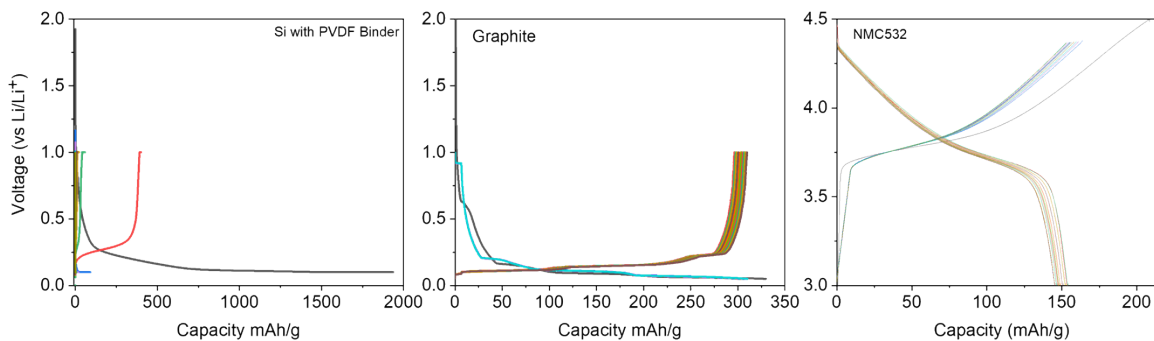


Figure 1. Voltage versus capacity data for the first 10 cycles in a half cell configuration.

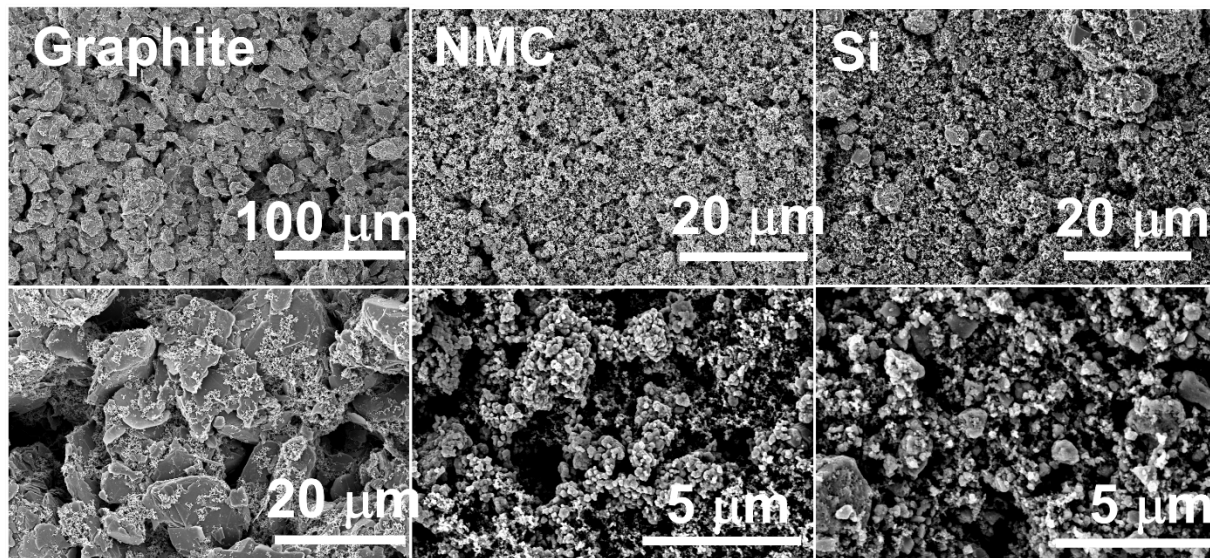


Figure 2. Representative SEM data collected for the cast electrodes showing porosity and good interconnecting networks.

Initially the adsorption behavior of PVDF on Si, graphite (Gr), and NMC, was evaluated by varying binder concentrations (0.25-10 wt%) of either A-PVDF or C-PVDF mixed with Si, Gr, or NMC in DMF. After mixing for 1 week, the resulting slurries were centrifuged, and the supernatants were measured via refractive index (RI) to estimate an adsorption profile as a function of binder concentration. RI is sensitive to minute changes in chemical structure and concentration and can be used to detect how much PVDF adsorbed onto the particles and how much remains in the supernatant. A 0.0001 change in RI data corresponds to a change in PVDF concentration of 0.21%. This concentration resolution is a function of the change in RI with concentration and is fundamentally limited by the PVDF RI. Note, the calibration curve did not change if the solution was centrifuged indicating good stability of the PVDF against precipitation. **Figure 3** presents the fraction of PVDF adsorbed as a function of PVDF in the slurry. The raw data is presented in **Figure S5** in RI of PVDF exposed to Si, Gr, or NMC particles as a function of starting wt% PVDF added to the slurry. From the calibration data the RI intensity decreases due to the addition of

PVDF (lower index of refraction) to the higher RI DMF. Therefore, an increase in RI signal for the electrodes corresponds to a decrease in PVDF concentration.

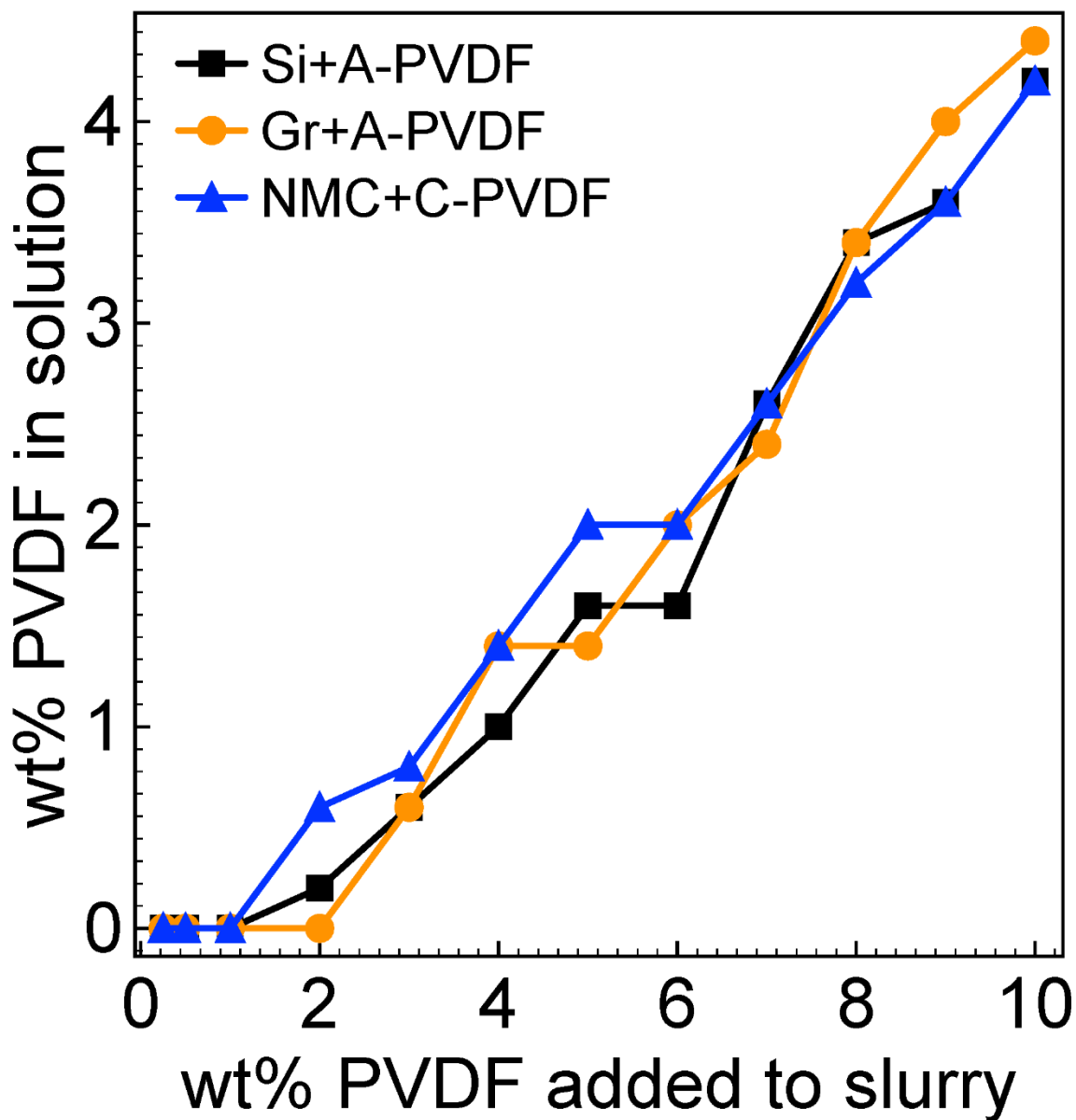


Figure 3: Amount of PVDF, either cathode or anode grade, in the supernatant of Si+A-PVDF (black squares), Gr+A-PVDF (orange circles), or NMC+C-PVDF (blue triangles) slurries plotted as a function of total amount of PVDF added to the slurry.

From the adsorption data, all the PVDF is bound to the surface of the electrode material when used in small concentrations; specifically, total adsorption on Gr and Si is seen when the

PVDF concentration was less than <1 wt% and total adsorption on NMC for binder concentrations < 2 wt%. At PVDF concentrations higher than 2 wt%, there is an increase in binder adsorption, but it is not totally absorbed onto the material. Indeed, only 55% of the PVDF, in a 10 wt% solution, is bound to the surface though Si+PVDF. This is surprising since slurries are often made with upwards of 25 wt% binder.⁷⁻¹⁸ This likely indicates at higher concentrations the binder is loosely bound or dynamic, engaging in polymer-polymer interactions. At low concentrations (< 2 wt%) all the binder is associated with the electrode material and is coincidentally in the concentration range typical for commercial electrodes.³¹ These results are consistent with X-ray absorption near edge spectroscopy (XANES) mapping, calorimetry, microprobe analysis, where graphite adsorbs only ~ 40% of the available PVDF, and the unattached PVDF forms discrete aggregates.^{3, 6, 19, 20}

Given the BET surface areas of the Si (25 m²/g) and Gr (5 m²/g) one might expect a 5x increase in PVDF adsorption on the silicon. Instead, the total binder saturation appears higher on the lower surface area graphite (2 wt%). This indicates the binder on Si is likely more isolated as discrete islands or much thinner than the comparable coating on Gr. Additionally, the NMC slurry adsorbs a similar concentration of PVDF as the Si despite the lower surface area (4.3 m²/g) indicating more binder per surface area which likely influences the structure investigated below.

To elucidate the polymer dynamics and structure of PVDF associated with Si, Gr, and NMC based electrodes, USANS and SANS were used to investigate the slurry structure as a function of shear from macroscale to nanoscale. Conceptually, the SANS measurements cover small length scales (6-200 nm) and describe species, like individual polymer chains, while USANS covers longer length scales associated with aggregates and agglomerates (up to 10 μm). In this way, the dynamics of the aggregate and agglomerate structures, as well as the interactions of single

PVDF chains, can be evaluated to reveal the main structural components that control electrochemical processes, such as lithium ion and electron diffusion.

Structure of PVDF-based slurries

Slurry morphology at 0 Hz

Rheology coupled ultra-small angle neutron scattering (rheo-USANS) was used to examine the slurry structure various length scales. Both USANS and SANS scattering curves (See Supporting Information, **Figure S6** and **S7**) were fit with a correlation length model (CLM). The CLM model (described in the Supplemental Section) estimates size, shape, and interconnectedness of the polymer-electrode aggregates. The black bounding boxes in **Figures 4, 5, and 6** denote visual representations of the USANS and SANS data directly derived from the CLM fit parameters. The cartoons at the top and bottom of **Figures 4, 5, and 6** depict the physical meaning and relative size of the slurry components and shows the relationship between SANS and USANS. The differently colored ellipses in the black bounding cubes in **Figures 4, 5, and 6** describe the aggregates—both number and size—where more ellipses equate to more aggregates. The severity of the overlap of the ellipses represents the size and number of agglomerates. The shape of the ellipses characterizes the shape of the aggregate. Expanded views of the ellipsoid data are shown in **Figures S8** and **S9**.

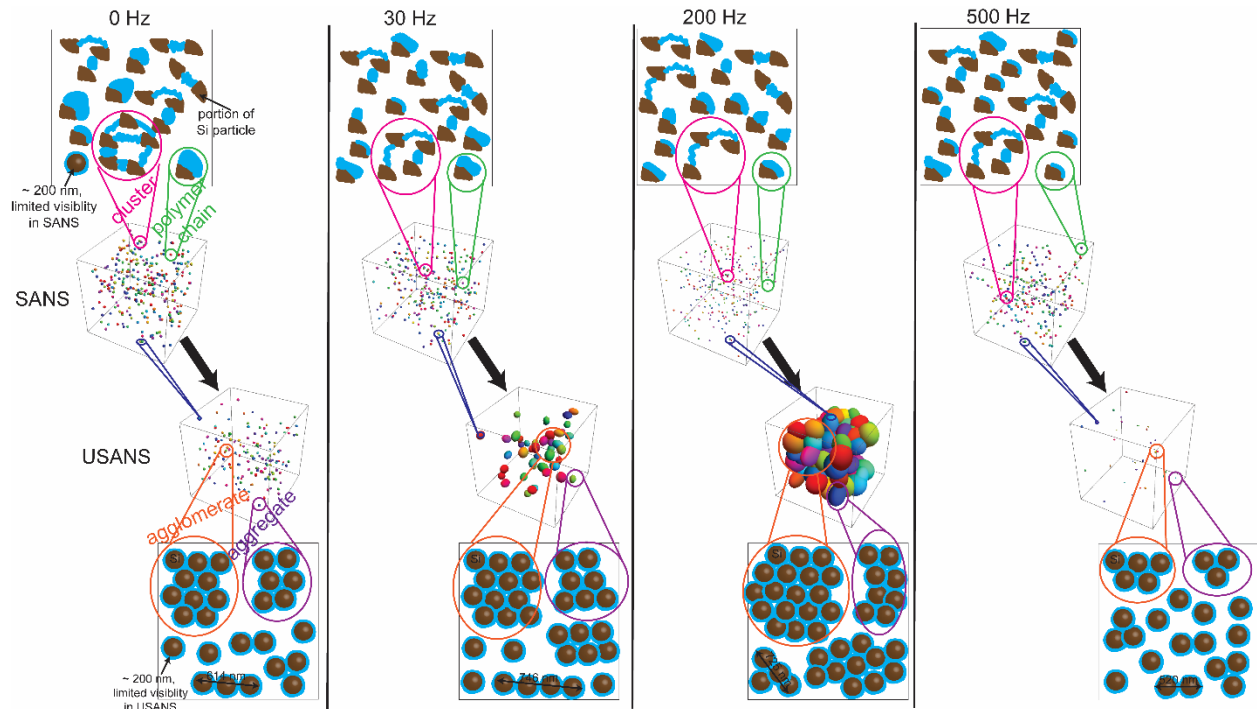


Figure 4: Schematic representation of structures probed by SANS and USANS for the Si+A-PVDF slurries at 0, 30, 200, and 500 Hz. For the USANS schematic, the number and size of the ellipses (represented by different colors) is directly derived from the C parameter of the CLM fit scattering curves while the amount of overlap of the ellipses represent the number and size of the agglomerates (A parameter). Each black bounding box contains the same volume of slurry and mass is conserved. Since USANS probes structures greater than 200 nm, the “white space” in some of the bounding boxes is comprised of sub-200 nm species. For the SANS schematic, the number and size of the ellipses (represented by different colors) represents the solvation of the polymer and is directly derived from the C parameter of the CLM fit scattering curves while the amount of overlap of the ellipses represent the number and size of the clusters (A parameter). Each black bounding box contains the same volume of slurry and mass is conserved. Since SANS probes structures greater than 6 nm, the “white space” in some of the bounding boxes may be composed of sub-6 nm species. The USANS (bottom) and SANS (top) cartoons show what the ellipsoids are physically and shows the cluster length size.

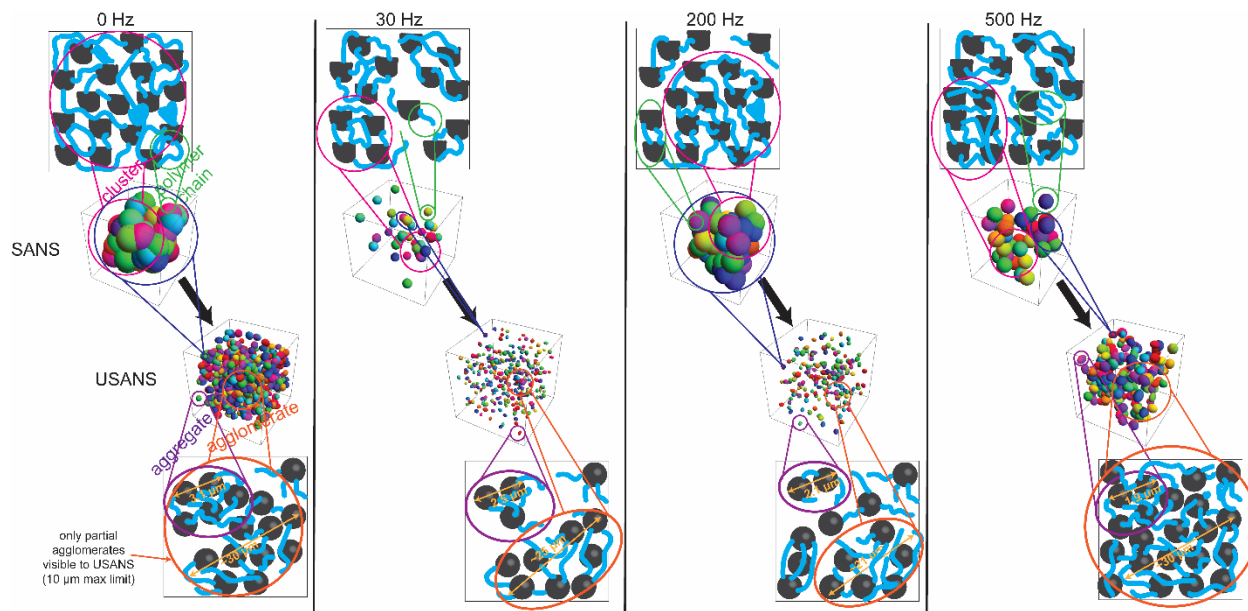


Figure 5: Schematic representation of structures probed by SANS and USANS for the Gr+A-PVDF slurries at 0, 30, 200, and 500 Hz. See **Figure 4** for details.

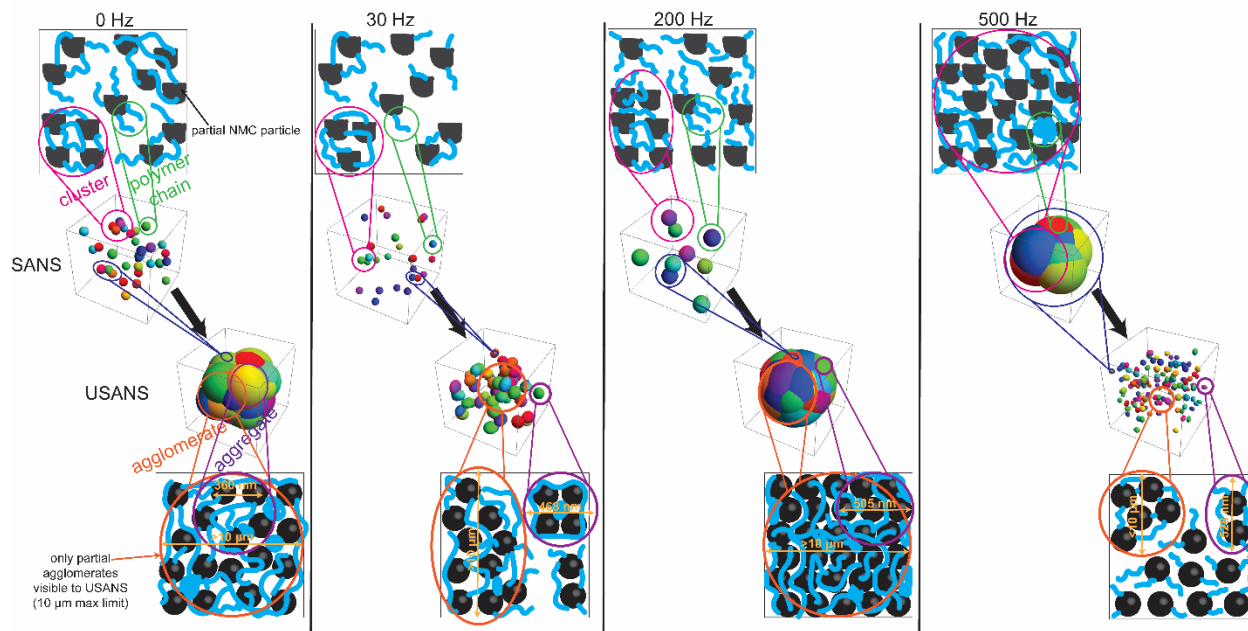


Figure 6: Schematic representation of structures probed by SANS and USANS for the NMC+C-PVDF slurries at 0, 30, 200, and 500 Hz. See **Figure 4** for details.

At rest, the Si+A-PVDF, Gr+A-PVDF, and NMC+C-PVDF slurries exhibit significant differences in the larger structural components (aggregates and agglomerates) of the slurry. The

agglomerates are the largest structural unit, which is on the order of 4-10 μm). The agglomerates are composed of aggregates, the second largest structural unit, which is on the order of 1-4 μm . The NMC slurry has the largest number and size of agglomerates by at least 2 orders of magnitude while the Si slurry has the fewest number of agglomerates by ~ 3 orders of magnitude. The Gr slurry has the intermediate level of agglomeration ($A=4.36 \times 10^{-5}$, Supporting Information). The smaller agglomerate size for Si, evidenced in **Figures 2**, is indicative of a highly dispersed polymer demonstrating that the A-PVDF interacts favorably with the silicon surface. The agglomerate size seems to scale inversely with surface area in that Si has the highest surface area at 25 m^2/g and the fewest number of agglomerates ($A=2.62 \times 10^{-4}$). The NMC has the largest number of agglomerates ($A=2.84 \times 10^{-7}$) while having the smallest surface area at 4.3 m^2/g . It is important to remember that a larger A value indicates a fewer number of agglomerates; i.e., NMC has the largest number of agglomerates.

However, the original size difference of the Si, NMC, and Gr particles cannot be ignored. The Si has a primary particle size of approximately 200 nm, while the Gr particles are, on average of 20 μm . Since USANS probes lengths up to 10 μm , primary particle size of most Gr particles is not measured. Therefore, the main parameter being probed is the polymer arrangement around the Gr particles. These larger particle size may lead to apparent increases in the agglomerate species in the Gr slurries. The average particle size of NMC is 478 nm, so USANS can probe the primary particle size. The severe agglomeration shown in the USANS data indicates that the particles are flocculating or being “glued” together by the PVDF where there are few discrete particles. On the other hand, the primary particle size of Si at 200 nm reaches the lower limit of what USANS can probe so USANS is likely determining multiple Si particles that have coalesced into aggregates and agglomerates.

The variation in the agglomeration behavior could also be due to differences in molecular weight of the C-PVDF or the A-PVDF. To investigate this the molecular weights of both PVDFs were evaluated by GPC. The weight average molecular weight (M_w) of C-PVDF and A-PVDF is 219,720 g/mol and 242,960 g/mol, respectively. Since a higher M_w would most likely result in larger agglomerates,^{32, 33} the dispersion of the Si+A-PVDF cannot be due to differences in molecular weight due to the similarity in the two polymers. Therefore, it is likely a morphological difference between the PVDF coating on the NMC versus the other active materials that causes the difference in agglomerations. For simplicity the A-PVDF and C-PVDF will be reduced to PVDF from this point forward.

These trends change when the aggregates of the slurries are observed. The Gr slurry has the largest number of aggregates by at least 2 orders of magnitude. Graphite adsorbs more PVDF than either Si or NMC as shown with the RI data, which is likely why there are more agglomerates in the Gr slurry although the size of the Gr particles could also contribute to the number aggregates. While NMC and Si adsorb the same amount of PVDF, the NMC slurry has the most agglomerates, by 2 orders of magnitude, but the fewest aggregates by 2 orders of magnitude (Supporting Information). This is likely due to the PVDF causing the NMC particles to coalesce, leaving few aggregate species in the slurry. Essentially, the NMC agglomerates are so large that there are limited species on the aggregate length scale; USANS shows that NMC is comprised of the larger agglomerate structures rather than the smaller aggregates structures. Since the Si particles are ~200 nm, there are more aggregate units (1-4 μm) than agglomerate units (4-10 μm). Si particles are prone to coalescence in solvent, but the fact that there are more aggregates than agglomerates in the Si slurries shows that the Si particles stay mostly discrete. One way this occurs is if the PVDF forms a conformal coating around the Si particles, sterically keeping the Si particles from touching

one another. Regardless, this points to a fundamental difference in the way the PVDF arranges itself around the active materials.

This difference can be further explored by examining the correlation length. The correlation length is a measure of the diameter of a cluster, which is the building block for an aggregate. Essentially, two or more clusters form an aggregate. The Gr+PVDF slurry has the largest correlation length at 3143 nm (See Supporting Information). This supports the literature in that the PVDF chains in a Gr slurry are elongated, linear, and reach into the liquid phase as a more elongated polymer chain will result in a larger correlation length.⁶ This larger correlation length indicates the Gr slurry having the largest and highest number of aggregates. This is consistent with the literature, which has previously shown that PVDF encapsulates or entangles many Gr particles, holding them in a matrix. Lastly, Gr adsorbs the most PVDF, as shown with the adsorption isotherms, and more material on the surface promotes larger particle diameters, thus corresponding larger correlation lengths.

The Si slurry has the intermediate correlation length at 614 nm, while the NMC slurry has the smallest cluster length at 360 nm. The NMC has the smallest correlation length likely because the agglomerate structures of NMC are so large that the signal from the clusters is overwhelmed by the signal from the agglomerate structures. Indeed, NMC is covered with a 5x thicker layer of PVDF than Si as calculated from the adsorption isotherms and BET surface area measurements.

The shape of the aggregate is relatively constant for all slurries—ellipsoidal—and does not seem to greatly affect the dynamics of the slurry at 0 Hz. The density of cluster packing is also similar for both Si and NMC slurries ($m=2.1-2.3$, Supporting Information). However, the cluster packing of the Gr slurry is 2x denser, which contributes to the Gr slurry having a larger

correlation length by about an order of magnitude and may be due to the plate like structure of graphite powder.

Slurry morphology at 30 Hz

Once the slurries are placed under shear, to simulate electrode slurry formation and casting, the structure of each slurry changes greatly as shown in **Figures 4, 5, and 6**. At 30 Hz, the Si slurry is the most agglomerated. This behavior has also been observed in Si slurries with polyimide and poly(acrylic acid) binders as is likely due to increased polymer-polymer entanglements induced by low shear forces.³⁴⁻³⁷ However, both the Gr and NMC slurries have a decrease in the number of agglomerates by at least a factor of 2 at the equivalent shear rate. Since both Si and Gr use A-PVDF as the binder, this difference is most likely due to the differences in adsorption of PVDF on the different active materials and polymer-polymer interactions reflected by the adsorption isotherms. It is unclear at this point what the difference in surface chemistries are that are responsible for these differences.

The Gr slurry has the largest number of aggregates at 30 Hz ($C=4.66 \times 10^6$), as compared to slurries containing Si and NMC, for the same reasons as described earlier. However, when the Gr slurry at 0 Hz and 30 Hz are compared, the Gr slurry at 30 Hz has an order of magnitude lower number of aggregates. As with the 0 Hz shear rate, the correlation length of the Gr slurry is the largest at 30 Hz ($L=2543$ nm). In contrast, the NMC slurry retains the smallest correlation length at 468 nm. However, on average, increasing the shear rate from 0 to 30 Hz does not greatly change the cluster or aggregate species in the slurries for the electrode materials investigated. Essentially, on the length scale of 200 nm-4 μ m, the slurry remains relatively unchanged. Additionally, increasing the shear rate seems to neither significantly influence the shape of the aggregate nor the

density of cluster packing. Indeed, the differences in the slurry dynamics arise from the changes in the agglomerate structure (4-10 μm).

Slurry morphology at 200 Hz

Both the Si and Gr slurry have fewer agglomerates as shear rate is increased from 30 Hz to 200 Hz (**Figures 5 and 6**). This is typical behavior of colloids in a viscoelastic (i.e., polymer) solution as the shear force breaks agglomerate structures and the PVDF chains align in the direction of shear.³⁸⁻⁴⁰ This behavior has been observed previously with Si slurries made with poly(acrylic acid).^{35-37, 41, 42} However, at 200 Hz, the NMC slurry has an increase in the number and size of agglomerates by 4 orders of magnitude when compared to 30 Hz. This is likely because PVDF forms a thick layer on NMC particles, as mentioned previously, that can encapsulate multiple NMC particles and remain porous.^{19, 20}

The Si slurry has fewer aggregates than the Gr slurry, which may be due to the PVDF forming a thinner layer on Si, due to the higher surface area and lower adsorption, resulting in a lower particle encapsulation thickness or coverage fraction. The correlation length trends are the same as they were with the slurries at 0 and 30 Hz. The shape of the aggregate and the density of cluster packing does not change with shear and still does not seem to influence the slurry dynamics.

Slurry morphology at 500 Hz

A further increase in shear rate to 500 Hz reveals that the slurry dynamics change drastically. It has been previously shown in the literature that PVDF adsorbs onto Gr, forming tendril-like chains that reach into the fluid phase, which “grabs” other Gr particles, so the Gr+PVDF complex resembles interconnected needle-like structure as shown via AFM and LFM.^{3,}

⁶ The correlation length of the Gr slurry at 500 Hz ($L=1869$ nm) is still an order of magnitude

larger than those of the Si and NMC slurries. This larger correlation length in the Gr slurry indicates that the clusters are elongated, and the polymer chains are outstretched into the solvent phase, which supports the aforementioned literature. The 500 Hz shear rate may cause enough turbulence in the slurry for the PVDF to encapsulate more Gr particles, resulting in an increase in the number of aggregates and agglomerates at 500 Hz.

Interestingly, at 500 Hz, the Si slurry becomes the most dispersed and is mostly comprised of sub-200 nm species as shown in **Figure 4** likely due to the high shear rates breaking up Si particle interactions. Again, this points to PVDF being an excellent dispersant of the silicon. In fact, it may disperse the silicon too well in that the PVDF isolates individual silicon particles from one another and there are no transport pathways for electrons in the electrode as there are discrete regions of PVDF and silicon particles. This hypothesis will be further investigated with EQSANS to probe the slurry on a smaller length scale and refractive index is used to investigate PVDF adsorption onto each active material (below).

The number of agglomerates in the NMC slurry decreases by 4 orders of magnitude as the shear rate is raised to 500 Hz. The effectiveness of a NMC slurry relies on the connected agglomerates and porous PVDF film. Since the NMC slurry has a larger number of agglomerates at 200 Hz, it is likely that the thinner electrode made with a 500 Hz shear rate would be electrochemically inferior to one made at 200 Hz.

Slurry structure at the nanoscale

To better elucidate the effect of PVDF adsorption on Si, Gr, and NMC, rheo-SANS was performed on each slurry at 0, 30, 200, and 500 Hz. The average size of Gr and NMC is larger than 200 nm, so SANS mostly probes the adsorbed PVDF and PVDF-PVDF agglomerates that are

less than 200 nm. Additionally, based on the size of the Si, Gr, and NMC particles, SANS can probe, at most, only partial portions of the particles as shown in **Figures 4, 5, and 6**. However, the Si primary particle size is 200 nm—right at the cross-over for SANS/USANS measurements, making the primary silicon particles virtually invisible to USANS/SANS. **Figures 4, 5, and 6** (top) present the visual representation of the SANS, where the extent of overlap now indicates the number of clusters and the number of ellipsoids indicates the discrete, non-solvated PVDF globules in the black bounding boxes. The individual ellipsoids in the USANS black bounding cube are comprised of overlapping ellipsoid clusters in the SANS black bounding box in **Figures 4, 5, and 6**.

Increasing the shear rate does not greatly affect the slurry dynamics at the 6-200 nm length scale, but the individual PVDF interaction with Si, Gr, and NMC are fundamentally different. The Si+PVDF slurry has the fewest number of clusters—by at least an order of magnitude—but has more discrete particles than any other slurries though the particles are much smaller than any of the particles in the other slurries (**Figures 4, 5, and 6**). The presence of these discrete particles is evidence that PVDF forms a thin coating around individual Si particles and the PVDF surrounding each particle does not interact with the PVDF coating on other particles as previously reported in the literature.⁴³⁻⁴⁵ Further, in conjunction with the adsorption isotherm data, this confirms that the PVDF is not bound to the silicon but instead acting as a dispersant to break up agglomerates in solution forming a unique structure in solution that likely conveys molecularly to the dried electrode.

This is certainly not the case for the Gr or NMC slurries where there are very large clusters of PVDF at all shear rates except for the 30 Hz shear rate. The large clusters are especially notable in the Gr slurry and further support the observation that the majority of the PVDF of a graphite

slurry resides at the Gr-Gr interface, “gluing” the Gr particles together in a large matrix. Similarly, the thick coating around the NMC particles can be observed by the presence of the large clusters. However, there is an order of magnitude fewer clusters in the NMC slurry than the Gr slurry as derived from the CLM fits of the curves and shown in Supporting Information, Table S6. This may indicate a couple of different scenarios: 1) there are fewer clusters because there are pores between each “globule” of PVDF, which would look like there were fewer PVDF clusters, 2) the PVDF on the NMC particles does not interact with PVDF on other NMC particles in the same way as the PVDF on the Gr particles interacts.

Together, the adsorption isotherm, USANS/SANS, and microscopy data point to the presence of a region of optimal PVDF binder coverage/morphology. The data indicates the Si+PVDF slurry is too homogeneous resulting in poor interconnects and resulting orphaned and trapped lithium after the first cycle. This orphaning is likely from the reaction occurring between the silicon and PVDF upon charge/discharge that prevents lithium transport from the silicon.⁴⁶ On the other end of the spectrum are the Gr and NMC slurries where the PVDF coating does not coat the entire surface of the particles, but where the PVDF stretches into the solvent phase and encapsulates many Gr and NMC particles, keeping the materials in a well-connected matrix and allows Li transport pathways to facilitate cycling through interzonal heterogeneity on the surface. This interzonal region entails the right mixture of surface heterogeneity with the binder such that the electrode is not completely passivated by a conformal binder coating.³⁴ Such an effect has been observed for polyacrylic acid based binders where surface heterogeneity is essential to ion transport for planar electrodes.⁴⁷ Similar heterogeneity was observed for polyimide based binders⁴⁸ and points to the passivating role of binders when not coated properly. Given the above results it would be reasonable to envision electrodes with sub-uniform coatings of PVDF may

engineer surface heterogeneity and the resulting lithium transport pathways that have hitherto been masked by the high binder loadings reported in the literature. Alternatively, changing the surface chemistry of the Si, through the introduction of PVDF-phobic surface sites, may build from the dispersing ability of PVDF and enable the correct surface heterogeneity to enable cycling.

Conclusion

It is often assumed that PVDF “does not work” for silicon-based electrodes, but there has not been conclusive evidence why PVDF is an inferior binder for silicon when compared to graphite and NMC. Generally, researchers cite that PVDF does not have enough mechanical integrity to support the swelling of the silicon anode upon cycling, but the reason behind this mechanical instability is not well understood. Through a combination of USANS, SANS, and refractive index measurements we show that a conformal layer of PVDF forms on individual silicon particles or small silicon aggregates, which causes the silicon slurry and electrode to be too homogeneous and the PVDF cannot form an interconnected matrix as it does on Gr and NMC. Furthermore, the PVDF on silicon makes a dense, conformal coating on the silicon, which may trap lithium ions after the first lithiation cycle. The observations herein show that if the surface of silicon can be modified in such a way as to promote a porous PVDF film on the particles and/or create an interconnected PVDF matrix to have a less homogeneous electrode, PVDF could potentially be a viable binder for silicon anodes.

Acknowledgements

The authors would like to thank Tim Armstrong of Steward Advanced Materials for the commercial sample of the NMC. This research (MKBT, BLA, GMV) was supported by the U.S. Department of Energy’s Vehicle Technologies Office under the Silicon Consortium Project,

directed by Brian Cunningham, and managed by Anthony Burrell. A portion of this research used resources at the Spallation Neutron Source, a DOE Office of Science User Facility operated by Oak Ridge National Laboratory (MD and LH). The small angle scattering measurements were done using the USANS and EQSANS instruments at the Spallation Neutron Source. This work benefited from the use of the SasView application, originally developed under NSF award DMR-0520547. SasView contains code developed with funding from the European Union's Horizon 2020 research and innovation programme under the SINE2020 project, grant agreement no. 654000. The authors thank Paul Dodson and Bill Aronoff for their invaluable help with the GPC. N.K. and A.K.N. thank Sumit Gupta and Siddhant Datta for assistance with EDXS measurements. This manuscript has been authored by UT-Battelle, LLC, under Contract DE-AC05-00OR22725 with the U.S. Department of Energy. The United States Government retains and the publisher, by accepting the article for publication, acknowledges that the United States Government retains a nonexclusive, paid-up, irrevocable, worldwide license to publish or reproduce the published form of this manuscript, or allow other to do so, for United States Government purposes. The Department of Energy will provide public access to these results of federally sponsored research in accordance with the DOE Public Access Plan (<http://energy.gov/downloads/doe-public-access-plan>).

Author Contributions

MKBT lead the experimental work, data analysis, and writing. BLA supervised the rheology and data analysis. RJK made and cycled the graphite electrode. JLT made and cycled the NMC electrode. RDM performed SEM characterizations. LH and MD assisted in the SANS/USANS data collection and analysis. DTH assisted with the Si production. NK performed BET and EDX

measurements. AKN assisted with editing and writing. GMV supervised the work, conceived the experiments, and lead the writing.

Associated Content

SEM/EDX, Refractive Index, USANS, SANS figures along with tables summarizing the fits to the USANS and SANS data are presented in the Supplemental Information Section. The Supporting Information is available free of charge at xxxxx.

References

1. Zhang, S. S.; Jow, T. R., Study of Poly(acrylonitrile-methyl methacrylate) as Binder for Graphite Anode and LiMn_2O_4 Cathode of Li-Ion Batteries. *J. Power Sources* **2002**, *109* (2), 422-426.
2. Zhang, X.; Ross, P. N.; Kostecki, R.; Kong, F.; Sloop, S.; Kerr, J. B.; Striebel, K.; Cairns, E. J.; McLarnon, F., Diagnostic Characterization of High Power Lithium-Ion Batteries for Use in Hybrid Electric Vehicles. *J. Electrochem. Soc.* **2001**, *148* (5), A463-A470.
3. Yoo, M.; Frank, C. W.; Mori, S.; Yamaguchi, S., Interaction of Poly(vinylidene fluoride) with Graphite Particles. 2. Effect of Solvent Evaporation Kinetics and Chemical Properties of PVDF on the Surface Morphology of a Composite Film and its Relation to Electrochemical Performance. *Chem. Mater.* **2004**, *16* (10), 1945-1953.
4. Wang, M.; Hu, J. Z.; Wang, Y. K.; Cheng, Y. T., The Influence of Polyvinylidene Fluoride (PVDF) Binder Properties on $\text{LiNi}_{0.33}\text{Co}_{0.33}\text{Mn}_{0.33}\text{O}_2$ (NMC) Electrodes Made by a Dry-Powder-Coating Process. *J. Electrochem. Soc.* **2019**, *166* (10), A2151-A2157.
5. Wang, M.; Dang, D. Y.; Meyer, A.; Arsenault, R.; Cheng, Y. T., Effects of the Mixing Sequence on Making Lithium Ion Battery Electrodes. *J. Electrochem. Soc.* **2020**, *167* (10), 100518.
6. Yoo, M.; Frank, C. W.; Mori, S., Interaction of Poly(vinylidene fluoride) with Graphite Particles. 1. Surface Morphology of a Composite Film and its Relation to Processing Parameters. *Chem. Mater.* **2003**, *15* (4), 850-861.
7. Erk, C.; Brezesinski, T.; Sommer, H.; Schneider, R.; Janek, J., Toward Silicon Anodes for Next-Generation Lithium Ion Batteries: A Comparative Performance Study of Various Polymer Binders and Silicon Nanopowders. *ACS Appl. Mater. Interfaces* **2013**, *5* (15), 7299-7307.
8. Hu, J. Z.; Wang, Y. K.; Li, D. W.; Cheng, Y. T., Effects of Adhesion and Cohesion on the Electrochemical Performance and Durability of Silicon Composite Electrodes. *J. Power Sources* **2018**, *397*, 223-230.
9. Jeena, M. T.; Lee, J. I.; Kim, S. H.; Kim, C.; Kim, J. Y.; Park, S.; Ryu, J. H., Multifunctional Molecular Design as an Efficient Polymeric Binder for Silicon Anodes in Lithium-Ion Batteries. *ACS Appl. Mater. Interfaces* **2014**, *6* (20), 18001-18007.
10. Liu, J.; Zhang, Q.; Zhang, T.; Li, J. T.; Huang, L.; Sun, S. G., A Robust Ion-Conductive Biopolymer as a Binder for Si Anodes of Lithium-Ion Batteries. *Adv. Funct. Mater.* **2015**, *25* (23), 3599-3605.
11. Magasinski, A.; Zdyrko, B.; Kovalenko, I.; Hertzberg, B.; Burtovyy, R.; Huebner, C. F.; Fuller, T. F.; Luzinov, I.; Yushin, G., Toward Efficient Binders for Li-Ion Battery Si-based Anodes: Polyacrylic Acid. *ACS Appl. Mater. Interfaces* **2010**, *2* (11), 3004-3010.

12. Nguyen, C. C.; Seo, D. M.; Chandrasiri, K.; Lucht, B. L., Improved Cycling Performance of a Si Nanoparticle Anode Utilizing Citric Acid as a Surface-Modifying Agent. *Langmuir* **2017**, *33* (37), 9254-9261.
13. Nguyen, C. C.; Yoon, T.; Seo, D. M.; Guduru, P.; Lucht, B. L., Systematic Investigation of Binders for Silicon Anodes: Interactions of Binder with Silicon Particles and Electrolytes and Effects of Binders on Solid Electrolyte Interphase Formation. *ACS Appl. Mater. Interfaces* **2016**, *8* (19), 12211-12220.
14. Wang, C.; Wu, H.; Chen, Z.; McDowell, M. T.; Cui, Y.; Bao, Z. A., Self-healing Chemistry Enables the Stable Operation of Silicon Microparticle Anodes for High-Energy Lithium-Ion Batteries. *Nat. Chem.* **2013**, *5* (12), 1042-1048.
15. Wang, Y. K.; Dang, D. Y.; Li, D. W.; Hu, J. Z.; Cheng, Y. T., Influence of Polymeric Binders on Mechanical Properties and Microstructure Evolution of Silicon Composite Electrodes During Electrochemical Cycling. *J. Power Sources* **2019**, *425*, 170-178.
16. Wang, Y. K.; Dang, D. Y.; Li, D. W.; Hu, J. Z.; Zhan, X. W.; Cheng, Y. T., Effects of Polymeric Binders on the Cracking Behavior of Silicon Composite Electrodes During Electrochemical Cycling. *J. Power Sources* **2019**, *438*, 226938.
17. Yoon, J.; Oh, D. X.; Jo, C.; Lee, J.; Hwang, D. S., Improvement of Desolvation and Resilience of Alginate Binders for Si-Based Anodes in a Lithium Ion Battery by Calcium-Mediated Cross-Linking. *Phys. Chem. Chem. Phys.* **2014**, *16* (46), 25628-25635.
18. Zhang, G. Z.; Yang, Y.; Chen, Y. H.; Huang, J.; Zhang, T.; Zeng, H. B.; Wang, C. Y.; Liu, G.; Deng, Y. H., A Quadruple-Hydrogen-Bonded Supramolecular Binder for High-Performance Silicon Anodes in Lithium-Ion Batteries. *Small* **2018**, *14* (29), 1801189.
19. Zhao, X. Y.; Niketic, S.; Yim, C. H.; Zhou, J. G.; Wang, J.; Abu-Lebdeh, Y., Revealing the Role of Poly(vinylidene fluoride) Binder in Si/Graphite Composite Anode for Li-Ion Batteries. *ACS Omega* **2018**, *3* (9), 11684-11690.
20. Yoo, M.; Frank, C. W.; Mori, S.; Yamaguchi, S., Effect of Poly(vinylidene fluoride) Binder Crystallinity and Graphite Structure on the Mechanical Strength of the Composite Anode in a Lithium Ion Battery. *Polymer* **2003**, *44* (15), 4197-4204.
21. Li, J. T.; Wu, Z. Y.; Lu, Y. Q.; Zhou, Y.; Huang, Q. S.; Huang, L.; Sun, S. G., Water Soluble Binder, an Electrochemical Performance Booster for Electrode Materials with High Energy Density. *Adv. Energy Mater.* **2017**, *7* (24), 1701185.
22. Wang, H. X.; Wei, D.; Zhang, B.; Ji, Z. K.; Wang, L. G.; Ling, M.; Liang, C. D., Epoxy Cross-Linking Enhanced the Toughness of Polysaccharides as a Silicon Anode Binder for Lithium-Ion Batteries. *ACS Appl. Mater. Interfaces* **2021**, *13* (31), 37704-37712.
23. Sethuraman, V. A.; Nguyen, A.; Chon, M. J.; Nadimpalli, S. P. V.; Wang, H.; Abraham, D. P.; Bower, A. F.; Shenoy, V. B.; Guduru, P. R., Stress Evolution in Composite Silicon Electrodes during Lithiation/Delithiation. *J. Electrochem. Soc.* **2013**, *160* (4), A739-A746.
24. Sinha, P.; Datar, A.; Jeong, C.; Deng, X. P.; Chung, Y. G.; Lin, L. C., Surface Area Determination of Porous Materials Using the Brunauer-Emmett-Teller (BET) Method: Limitations and Improvements. *J. Phys. Chem. C* **2019**, *123* (33), 20195-20209.
25. Brandl, G.; Georgii, R.; Haussler, W.; Muhlbaauer, S.; Boni, P., Large Scales-Long Times: Adding High Energy Resolution to SANS. *Nucl. Instrum. Methods Phys. Res.* **2011**, *654* (1), 394-398.
26. Arnold, O.; Bilheux, J. C.; Borreguero, J. M.; Buts, A.; Campbell, S. I.; Chapon, L.; Doucet, M.; Draper, N.; Leal, R. F.; Gigg, M. A.; Lynch, V. E.; Markvardsen, A.; Mikkelsen, D. J.; Mikkelsen, R. L.; Miller, R.; Palmen, K.; Parker, P.; Passos, G.; Perring, T. G.; Peterson, P. F.; Ren, S.; Reuter, M. A.; Savici, A. T.; Taylor, J. W.; Taylor, R. J.; Tolchenoy, R.; Zhou, W.; Zikoysky, J., Mantid-Data Analysis and Visualization Package for Neutron Scattering and μ SR experiments. *Nucl. Instrum. Methods Phys. Res.* **2014**, *764*, 156-166.
27. Doucet, M.; Cho, J. H.; Alina, G.; Bakker, J.; Bouwman, W.; Butler, P.; Campbell, K.; Cooper-Benun, T.; Durniak, C.; Forster, L.; Gonzales, M.; Heenan, R.; Jackson, A.; King, S.;

- Kienzle, P.; Krzywon, J.; Nielsen, T.; O'Driscoll, L.; Potrzebowski, W.; Ferraz Leal, R.; Rozycko, P.; Snow, T.; Washington, A. *SasView*, 5.0; Zenodo: 2019.
28. Carpenter, J. M.; Agamalian, M.; Iop, Aiming for the Theoretical Limit of Sensitivity of Bonse-Hart USANS Instruments. In *International Conference on Neutron Scattering 2009*, 2010; Vol. 251.
 29. Agamalian, M.; Heroux, L.; Littrell, K. C.; Carpenter, J. M.; Iop, Progress on the Time-of-Flight Ultra Small Angle Neutron Scattering Instrument at SNS. In *22nd Meeting of the International Collaboration on Advanced Neutron Sources*, 2018; Vol. 1021.
 30. Zhao, J. K.; Gao, C. Y.; Liu, D., The Extended Q-range Small-Angle Neutron Scattering Diffractometer at the SNS. *J. Appl. Crystallogr.* **2010**, *43*, 1068-1077.
 31. Cholewinski, A.; Si, P.; Uceda, M.; Pope, M.; Zhao, B., Polymer Binders: Characterization and Development toward Aqueous Electrode Fabrication for Sustainability. *Polymers* **2021**, *13* (4), 631.
 32. Akay, G., Flow-Induced Phase Inversion Agglomeration-Fundamentals and Batch Processing. *Polym. Eng. Sci.* **1994**, *34* (11), 865-880.
 33. Linardos, S.; Zhang, Q.; Alcock, J. R., An Investigation of the Parameters Effecting the Agglomerate Size of a PZT Ceramic Powder Prepared with a Sol-Gel Technique. *J. Eur. Ceram. Soc.* **2007**, *27* (1), 231-235.
 34. Burdette-Trofimov, M. K.; Armstrong, B. L.; Heroux, L.; Doucet, M.; Sacci, R. L.; Veith, G. M., Structure and dynamics of small polyimide oligomers with silicon as a function of aging. *Soft Matter* **2021**, *17* (33), 7729-7742.
 35. Burdette-Trofimov, M. K.; Armstrong, B. L.; Murphy, R., P.; Heroux, L.; Doucet, M.; Rogers, A. M.; Veith, G. M., Probing Clustering Dynamics between Silicon and PAA or LiPAA Slurries under Processing Conditions *ACS Appl. Polym. Mater.* **2021**, *3* (5), 2447-2460.
 36. Burdette-Trofimov, M. K.; Armstrong, B. L.; Murphy, R., P.; Heroux, L.; Doucet, M.; Trask, S. E.; Rogers, A. M.; Veith, G. M., Role of Low Molecular Weight Polymers on the Dynamics of Silicon Anodes During Casting. *ChemPhysChem* **2021**, *22* (11), 1049-1058.
 37. Burdette-Trofimov, M. K.; Armstrong, B. L.; Rogers, A. M.; Heroux, L.; Doucet, M.; Yang, G.; Phillip, N. D.; Kidder, M. K.; Veith, G. M., Understanding Binder-Silicon Interactions During Slurry Processing. *J. Phys. Chem. C* **2020**, *124* (24), 13479-13494.
 38. Barnes, H. A., A Review of the Rheology of Filled Viscoelastic Systems. *Rheol. Rev.* **2003**, 1-36.
 39. Morris, E. R.; Cutler, A. N.; Ross-Murphy, S. B.; Rees, D. A., Concentration and Shear Rate Dependence of Viscosity in Random Coil Polysaccharide Solutions. *Carbohydr. Polym.* **1981**, *1* (1), 5-21.
 40. Scott Blair, G. W.; Hening, J. C.; Wagstaff, A., The Flow of Cream through Narrow Glass Tubes. *J. Phys. Chem.* **1939**, *43* (7), 853-864.
 41. Burdette-Trofimov, M. K.; Armstrong, B. L.; Weker, J. N.; Rogers, A. M.; Yang, G.; Self, E. C.; Armstrong, R. R.; Nanda, J.; Veith, G. M., Direct Measure of Electrode Spatial Heterogeneity: Influence of Processing Conditions on Anode Architecture and Performance. *ACS Appl. Mater. Interfaces* **2020**, *12* (50), 55954-55970.
 42. Armstrong, B. L.; Hays, K. A.; Ruther, R. E.; Hawley, W. B.; Rogers, A.; Greeley, I.; Cavallaro, K. A.; Veith, G. M., Role of silicon-graphite homogeneity as promoted by low molecular weight dispersants. *J. Power Sources* **2022**, *517*, 230671.
 43. Hong, M. H.; Lee, S.; Choi, S.; Mun, J., Polyimide Binder for a High-Energy-Density Composite Anode Electrode with Graphite and Silicon. *J. Electroanal. Chem.* **2020**, *871*, 114317.
 44. Huang, W. B.; Wang, W.; Wang, Y.; Qu, Q. T.; Jin, C. C.; Zheng, H. H., Overcoming the Fundamental Challenge of PVDF Binder Use with Silicon Anodes with a Super-Molecular Nano-Layer. *J. Mater. Chem. A* **2021**, *9* (3), 1541-1551.
 45. Hwang, S. S.; Sohn, M.; Park, H. I.; Choi, J. M.; Cho, C. G.; Kim, H., Effect of the Heat Treatment on the Dimensional Stability of Si Electrodes with PVDF Binder. *Electrochim. Acta* **2016**, *211*, 356-363.
 46. Han, B. H.; Piernas-Munoz, M. J.; Dogan, F.; Kubal, J.; Trask, S. E.; Bloom, I. D.; Vaughey, J. T.; Key, B., Probing the Reaction between PVDF and LiPAA vs Li₇Si₃: Investigation of Binder Stability for Si Anodes. *J. Electrochem. Soc.* **2019**, *166* (12), A2396-A2402.

47. Browning, K. L.; Sacci, R. L.; Doucet, M.; Browning, J. F.; Kim, J. R.; Veith, G. M., The Study of the Binder Poly(acrylic acid) and Its Role in Concomitant Solid–Electrolyte Interphase Formation on Si Anodes. *ACS Appl. Mater. Inter.* **2020**, *12* (8), 10018-10030.
48. Burdette-Trofimov, M. K.; Armstrong, B. L.; Heroux, L.; Doucet, M.; Márquez Rossy, A. E.; Hoelzer, D. T.; Kanbargi, N.; Naskar, A. K.; Veith, G. M., Competitive adsorption within electrode slurries and impact on cell fabrication and performance. *J. Power Sources* **2022**, *520*, 230914.

Morphology of PVDF around electroactive materials

